Mesh Addition Based on the Depth Image (MABDI)

by

Lucas E. Chavez

B.S., Mechanical Engineering

New Mexico Institute of Mining and Technology, 2009

THESIS

Submitted in Partial Fulfillment of the

Requirements for the Degree of

Master of Science

Mechanical Engineering

The University of New Mexico

Albuquerque, New Mexico

December, 2016

Acknowledgments

Mesh Addition Based on the Depth Image (MABDI)

by

Lucas E. Chavez

B.S., Mechanical Engineering
New Mexico Institute of Mining and Technology, 2009

M.S., Mechanical Engineering, University of New Mexico, 2016

Abstract

Many robotic applications, especially those whose goal is to aid or assist through human-robot interaction, utilize a rich map of the world for reasoning tasks such as collision detection, path planning, or object recognition. Such a map, and the method used to produce it, must take into consideration real-world constraints. Most mesh-based mapping algorithms resemble a "black box" and do not provide a mechanism to close the loop and make decisions about the incoming information. MABDI leverages the global mesh by finding the difference between what we expect to see and what we are actually seeing, and using this to classify the incoming measurements as novel or not. This allows the surface reconstruction method to be run only on data that has not yet been represented in the global mesh. The result is an algorithm that becomes computationally inexpensive once the environment is known, but still can incorporate new objects into the model.

Contents

Contents

3   Approach   **22**

A   MABDI code   **31**

References   **46**

Chapter 1

Introduction

1.1 Overview

Many robotic applications, especially those that involve human-robot interaction, often require a rich representation of the environment in order to perform such behavior as path planning and obstacle avoidance. In general, a rich representation, or map, is useful for providing situational awareness to an autonomous agent. A map is also important for applications such as teleoperation [1].

In robotics, map building in an unknown environment is referred to as the Simultaneous Localization and Mapping (SLAM) problem [2]. This label describes the fact that a methodology which solves the SLAM problem must simultaneously locate the robot in the environment as well as map the environment. The focus of this work is the mapping aspect of the SLAM problem. Fig. 1.1 gives a visualization of the goal.

The methodology to build a map is a continuously evolving subject in the field of robotics and computer graphics. Well known works of map building methods be-
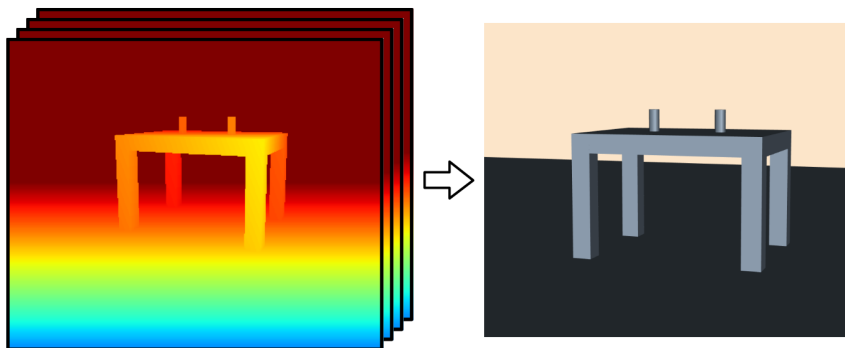
Figure 1.1: Goal is to create a map from depth images.

gan to be seen around 1987 [3]. Since then, the methods and the representations themselves have continued to evolve at an impressive rate. Growth in this field of research has been fueled by continuous advances in computing and sensing technologies. Over the years, sensors have continued to generate measurements at higher rates, higher resolution, and lower cost. RGB-D sensors are a new category of sensor that have recently gained extensive popularity in the robotics community due to their affordability and ability to generate a rich amount of data.

1.1.1 RGB-D Sensors

The popularity of RGB-D sensors began with the release and commercialization of the Kinect™ by Microsoft. The arrival of the Kinect brought with it an inexpensive depth sensor that uses an active range system to generate a depth map of a given environment [4]. The Kinect and similar sensors, have come to be called RGB-D sensors. This class of sensors provide images which include both visual (RGB) and depth (D) values. Several works have taken advantage of this sensor technology in scenarios such as environmental mapping [5], 3D reconstruction [6], gesture recognition [7], and altitude control of aerial vehicles [8].

RGB-D sensors generally provide data at 30 frames per second and 640×480 resolution. Consequently, methods that use RGB-D data must handle over 9 million pixel values per second, if only using the depth information (D), and over 18 million if using both color (RGB) and depth (D). The magnitude of the amount of data output from RGB-D sensors creates the need for mapping methods that are computationally inexpensive and also influences the type of data structure used to store the map.

1.1.2   Maps

There are different types of data structures that can define a map. All types have both intrinsic characteristics that impact the algorithms that generate them and constraints that must be considered for real-world applications. In addition, we are concerned with rich representation types, in contrast to sparse representation types [9], because rich types have the most use in applications such as human-robot interaction.

Table 1.1: Comparison of constraints for different map types.

	Supported	Computationally Inexpensive	Low Memory Requirement
Point Clouds	x	x	-
Surfels	-	x	x
Implicit Functions	x	-	-
Mesh	x	x	x

When considering which type of map is best for real-world applications, we must consider the constraints imposed by each type:

- Supported - Is there software, tools, research, algorithms, etc., for this type of map?

- Computationally Inexpensive - Can the algorithms run quickly on low cost computers (rather than specialized hardware)?

- Low Memory Requirement - Can the algorithms run on hardware with a standard amount of RAM?

Table 1.1 compares the constraints of common map types. We can see, in general a mesh type map satisfies real-world constraints. Additionally, meshes have been used extensively by the gaming and graphics communities, and so benefits from an incredible amount of continued research and advances in hardware such as Graphics Processing Units (GPUs).

1.2   Goal

The goal of this work is to develop a mapping algorithm that can gracefully utilize the amount of data output from an RGB-D sensor. Additionally, the algorithm will make use of software tools and hardware that have been developed for mesh data structures. The algorithm will be able to make intelligent decisions using the data it receives based on the knowledge it has been building about the environment. The decisions will be driven by the leveraging the difference between what the algorithm is actually seeing and what it expects to see. The decisions will be generated using computationally inexpensive computer vision methods.

1.3   Contribution

MABDI's contribution to the state-of-the-art in mesh based environmental mapping methods is to close the loop of the algorithmic structure used by current methods.

Current mesh mapping techniques can be described as "black box" methods. The general algorithmic structure of these "black box" methods follows the same pattern, which can be thought of as a pipeline. Data comes in from the sensor, those measurements are used to create a mesh, and then that mesh is appended to a global mesh. Fig. 1.2a shows this pipeline. We can then compare that pipeline to the pipeline used in MABDI, which is shown in Fig. 1.2b. In both figures we can see the "Create Mesh from Input" component. The input to this component is different for "black box" methods and MABDI. "Black box" methods input all data from the sensor into the mesh creating component whereas MABDI only inputs data identified to be from the unknown parts of the environment. This reduces the computational cost of the mesh creating component and results in a global mesh that does not have redundant mesh elements. Redundant mesh elements are an inherent problem of "black box" methods and are typically removed using computationally expensive post processing of the global mesh. MABDI simply does not create redundant elements to begin with. Reduced computational cost and a global mesh that is inherently free of redundant elements is MABDI's contribution.
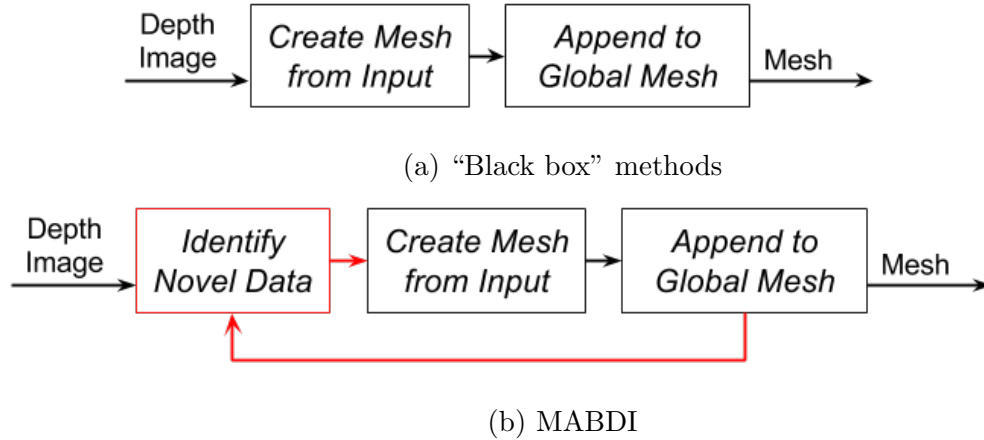

(a) "Black box" methods

(b) MABDI

Figure 1.2: Algorithmic structure of "black box" methods (a) compared to MABDI (b). Contribution of MABDI to the state-of-the-art shown in red

Chapter 2

Related Works

A major problem in robotics has been and continues to be: How can we create the "best" representation of an unknown environment? There are two main communities of researchers who been working on developing algorithms and methods to answer precisely this question. They are the robotics community and the computer graphics community, but each community has a slightly different motivation for solving this problem. The robotics community is concerned with developing a real-time solution for generating representations in large environments. In the literature, large environments usually range in size from multi-room office spaces to a few square miles on city streets. These representations are used by both fully autonomous and tele-operated systems. The common name which is used by the robotics community for this problem is Simultaneous Localization and Mapping or SLAM. The name SLAM refers to the problem of mapping and locating a robot in an unknown environment. Early methods generated very sparse representations of the world, as time and sensor technology progressed the representations became denser. A dense representation is desired for any system that must have good situational awareness of its environment. The computer graphics community is concerned with generating high quality representations of small environments. In the literature, small environments usually

range in size from a cubic meter to room size. They generally refer to the problem as surface reconstruction. These representations are used by augmented reality, computer game object creation, 3D printing, and other applications. In the following sections we will trace the development of representation generating methods in both communities.

2.1   SLAM

The problem of SLAM has been a primary focus of the robotics community for more than 25 years. A complete solution to the SLAM problem must be able to generate a representation of an unknown environment and track the robot in this new representation. In this body of literature the act of generating a representation is referred to as mapping. A good overview of the problem can be found in [10] and [11]. Each solution is designed to consider the goal application, type of sensor, computational constraints, and memory limits. All these factors influence the researcher's choice of which type of representation to use for the mapping procedure. In 2002 Thrun wrote a famous survey [2] of the SLAM literature which categorized existing algorithms on many traits including the representation. The representation choice of prior work can be roughly categorized into three types. The first type is characterized by some sort of list of 2D or 3D points and are usually considered to be sparse representations. Common names for these types are landmark locations and point clouds. The second type is considered to be more volumetric based and is often times considered to be a dense representation. Common names for these types are occupancy grid and Truncated Signed Distance Function (TSDF). The last type has the characteristic of being a surface representation and is also considered to be a dense representation. Common names for these types are surfels and mesh. In the following sections we will trace the history of each of the three types of representation that are seen in the

SLAM literature.

2.1.1   Point Locations

One of the most well known and earliest solution to the SLAM problem, which uses a point location representation, was proposed by Smith et al. in 1990 [12]. The mathematical framework that he created was the origin of a family of solutions based on the Extended Kalman Filter (EKF). The representation he chose was simply a list of 2D landmark locations. Each location was part of a state matrix which was estimated at every iteration. A list of landmark locations was chosen because it allowed the method to have a low computational cost and use a small amount of memory, important factors in the days of early computing. There have been many improvements to the family of SLAM solutions which generate a list of point locations since Smith's work. One of the first practical implementations on a real robot was done by Thrun in 1998 [13]. In this work the SLAM problem was posed in an Expectation Maximization (EM) framework which is similar to the EKF framework in that landmark locations are saved in a state vector which is estimated at every iteration. In Thrun's work an occupancy grid map is generated as a post processing step from sonar measurements. The results showed that their representation could become more accurate over time by using new observations to improve the current estimate. This a highly desired ability of any representation generation method. The next step was the ability of these methods to include a loop closure procedure. A loop closure procedure was proposed by Gutmann in 1999 [14]. The key ability of the method was it could recognize when the robot was revisiting a prior location and adjust the entire representation with the constraint that the two points must coincide. In 2001 Dissanayake et al. [9] derived three theorems to theoretically prove the convergence of the SLAM problem. Their test platform used a millimeter-wave radar mounted on a vehicle and generated a list of 2D landmark locations.

In 2001 Thrun et al. [15] cast the SLAM problem using particle filter techniques. Their results generated a 2D map and showed an increased robustness and lower computational cost than prior methods. One of the key disadvantages of methods up to this point was that complexity scaled quadratically with the number of landmark locations. In 2002 Montemerlo et al. [16] created a SLAM solution named FastSLAM, which was able to handle a much larger number of landmarks. They showed results with maps containing more than 50,000 points. Then, SLAM solutions using point locations became much more directed towards 3D.

Some of the first interesting works that represented the world as a list of 3D point locations were done by Thrun et al. in 2000 [17], Liu and Emery in 2001 [18], and Hähnel et al. in 2003. In these works the 2D landmark locations and robot position were estimated using techniques from Thrun's past work [13]. Once this had been done the 3D laser scan data was simply appended to each estimated robot location. Then, a mesh was created by post processing the 3D point cloud. Their works utilized the fact that the laser collected the data in an incremental manner and simply connected neighboring 3D points. Finally, the mesh was simplified by looking for large planar sections and merging the corresponding mesh elements. One of the first SLAM solutions which used a single camera to generate a list of 3D points was done by Davison in 2003 [19]. Here he used a single camera to generate a very sparse list of 3D points. This method was limited to small environments. Future advances allowed representations of larger environments. In 2003 Thrun et al. [20] created a SLAM procedure which did not rely on having a structured environment and was applied to mapping large mines. In 2004 Howard et al. [21] created a SLAM system based on a Segway platform equipped with a 3D laser which could map areas of roughly 0.5 km on each side. One of the results showed a map with approximately 8 million points. In 2006 Cole and Newman [22] continued work in large-scale SLAM by increasing robustness and also generated maps with many 3D points using a laser sensor. In 2007 Clemente et al. created a large-scale SLAM system that used a single

camera. The system had an advanced loop closing procedure based on visual features and created large maps of 3D points. In 2001 Klein and Murray [23] developed a SLAM solution which used a single camera. The uniqueness of their method was the algorithmic structure. Their SLAM solution consisted of two separate processes: a tracking process and a map building process. This algorithmic structure has become very common in many current SLAM solutions because of the advances in pose estimation technology. Klein and Murray were able to get very good results for a small environment and showed Augmented Reality (AR) applications. Many of the future advances of SLAM solutions, which generated 3D point sets, dealt with camera systems [24, 25, 26] and improved speed and robustness. Many of the most current methods that produce a list of points are systems who use a relatively new type of sensor named a RGB-D sensor. One good example is a work that was produced in 2011 by Engelhard et al. [27]. In this work they used an algorithm named the Iterative Closest Point (ICP) [28] to align point clouds coming from the RGB-D sensor into a large colored point cloud. The resulting maps were visually impressive. However, the map could not be adapted to new information and was not well suited for other applications, such as obstacle avoidance. These limitations are inherent in maps that consist of lists of points.

2.1.2 Volumetric

Many SLAM solutions generate a 2D volumetric representation of the world because they are especially advantageous in dealing with noisy sensors. Two of the first major works that generated a 2D volumetric representation were done in 1998 by Yamauchi et al. [29] and Schultz et al. [30]. These works generated a 2D occupancy grid, which is a type of volumetric representation. Here the environment was divided into a 2D grid. Each square of the grid contained the probability that it was occupied with an object. All squares would be updated iteratively based on the current sensor readings.

Occupancy grids, like any other volumetric-based representation, are limited by the amount of available memory. In 2002 Biswas et al. [31] extended occupancy grid methods by allowing dynamic environments. This was done by looking at past "snapshots" of the map. In 2004 Eliazar and Parr [32] continued the advancement by decreasing computational cost and implemented a loop closure method.

There have been a few impressive SLAM solutions that generate a 3D volumetric representation. There are three major works that generated a result very similar to a 3D occupancy grid, which was saved as in a octree data structure [33, 34, 35, 36]. Each work had a slightly different name and procedure for generating the representation, but in general the representations divided the environment into cubes and had a scalar value representing the belief of a surface being there. Octrees were used to save memory by only having a fine resolution of cubes at places where there was a surface. There are many advantages to a 3D occupancy grid representation. The representation is well suited for obstacle avoidance and path planning applications. Also, the representation is very adaptable to new information. The major disadvantage is that the representation can not be visualized immediately. In order to render, an image must be generated at each desired viewpoint by ray tracing the volume. This can be a problem when using such method for applications such as teleoperation due to the computational cost of rendering. The current state of the art for generating a volumetric representation was done by Newcombe et al. in 2011 [6]. Their system used a RGB-D sensor and generated a 3D voxelized grid Truncated Signed Distance Function (TSDF) of the environment. For this type of representation each cube contains the value of the distance to the nearest surface. The sign of the value is based on which side of the surface the cube is relative to the sensor. This work has been the most capable at dealing with extremely noisy data and dynamic scenes. However, due to memory constraints the method can only represent environments that are about the size of a 4m cube. Also, it must be ray traced in order to be visualized.

2.1.3   Surface

One of the first major works that created a surface representation of the environment in real-time was done by Martin and Thrun in 2002 [37]. Their method utilized an EM framework to fit plane models to 3D point cloud data. Polygon mesh elements were then easily assigned to each plane. The main drive behind this work was to generate a map of the environment that uses a small amount of memory. Their method worked well for structured environments. One of the major limitations of their method, and other methods that only mesh large planar sections, is that the representation will only consist of planar sections and not capture the fine detail of the environment. In 2004 Viejo and Cazorla [38] developed a methodology for generating a mesh that can contain more information of the environment than large planar sections. Due to this ability, they termed their method to be "unconstrained." Essentially their method was based on a 3D Delaunay triangulation algorithm. Giesen surveyed Delaunay triangulation methods in [39]. Viejo and Cazorla were not able to obtain real-time results and, in fact, it has been seen that it is extremely difficult to run a 3D Delaunay triangulation in real time because of the numerous distance calculations required. One of the next major advances came from Weingarten and Siegwart in 2006 [40]. Their work also created a mesh that was only capable of capturing large planar surfaces. However, they showed increased robustness. In 2007 Pollefeys et al. [41, 42] developed a large urban mapping system consisting of a vehicle and eight camera systems. The processing was carried out by multiple CPUs and optimized for speed with Graphics Processing Unit (GPU) calculations. In their work they used the camera systems to generate a set of depth maps. This set was then reduced using their depth map fusion method. The method combined multiple depth maps to reject erroneous depth estimates and remove redundancy from the data, resulting in a more accurate and reduced set of depth maps. The reduced set was then used by a triangulation procedure to create a mesh of the environment. The mesh generation

procedure was based on a work from 2002 by Pajarola et al. [43]. This method defines a mesh in the depth image. It starts from a very coarse mesh and continues to refine in areas of the depth image based on a confidence criteria. In the work of Weingarten and Siegwart, these meshes that are defined for each fused depth image are then checked for overlaps and duplicates are removed to make a single large mesh. One of the major drawbacks of this approach is that the output mesh can not be adapted by measurements that come from revisited parts of the scene. Another major advancement came in 2008 from Poppinga et al. [44]. In this work they used a Time of Flight (ToF) camera to generate a mesh representation of the large planar structures in the environment. Here they also develop a procedure to determine a mesh in a depth image. They leverage the structure of the depth image to make the method computationally inexpensive. In their work they simply append the meshes that are created from each depth image into a global coordinate system. They obtain very good results from a simple method. However, the method is not adaptive to new information. Also, a mesh is created for each depth image instead of updating and maintaining a global mesh. A major advancement came from work done by Newcombe and Davison in 2010 [45]. In this work they designed a method to create a mesh reconstruction from a single video camera. Their method used Structure From Motion (SFM) to obtain a sparse point cloud of the scene. Then an implicit function was fit to the point cloud using the methodology of Ohtake et al. [46]. A bundle of depth maps is then selected. From the bundle a single reference depth image is selected and a "base" model is constructed by sampling the implicit surface for vertices in the reference frame. The neighboring frames are used to better the "base" model and create a more accurate mesh. Each reference frame has its own mesh and all the meshes are put into a global coordinate system. Duplications are then detected and removed. Again, the representation is not adaptive to new information. In 2010 Stühmer et al. [47] generated very accurate depth maps from several color images in real-time. They showed very impressive results but their

method was not designed to maintain a representation in a global coordinate frame.

The next major advances in methods that generated surface representations of the environment, were based on RGB-D sensors. This type of sensor has become very popular since the release of the Kinect from Microsoft that was the first mass produced RGB-D sensor of its kind. RGB-D sensors are inexpensive and produce noisy 640x480 depth images at 30Hz. The RGB-D sensor has excited the robotics community because this has been the first time that depth data has been so readily accessible from such an inexpensive sensor. Therefore, these methodologies must be able to quickly deal with very high rates of information. One impressive work came from Henry et al. in 2012 [48]. In this work they designed a system that used a RGB-D sensor to build a map made of surfels (Surfels are circular disks which have a particular position and orientation and also a radial size based on confidence.). In order to generate and maintain the surfel map they used the work of Weise et al. [49]. The map consists of a large number of surfels. The surfel map can be updated given new registered depth images from the sensor. Decisions are made how to handle each measurement in the depth image based on the difference between an expectation generated using the current map and the actual readings from the sensor. Rendering a surfel map requires special methods [50] and is difficult to use in applications such as obstacle avoidance.

One of the next major advances is a highly-related work that was published by Whelan et al. in 2012 [51] and more recently in 2013 [52]. The system they developed was named Kintinuous and was able to produce a high quality mesh representation of the environment. Their hybrid system utilized the KinectFusion method [6] of Newcombe et al. to create a volumetric representation of the portion of the environment in front of the sensor. As the sensor moves, portions of the environment that leave the volume in front of the sensor are ray cast and turned into a mesh. They obtain very impressive results but also mention a limitation of their system for future

work. The limitation is that the mesh can not be updated once created, which is an issue when revisiting parts of the environment that may have changed. One of the most impressive current works which has an adaptable mesh came from Cashier et al. in 2012 [53]. In this work, they were able to generate and update a mesh with new measurements from a ToF sensor. They used the difference between the existing model and the actual measurements to decide whether to adapt the mesh or add new elements. The mesh topology was not adaptive to the environment and their experiments only showed results of mapping a single flat wall with no robot movement. The system needs to be tested for object addition and removal.

2.2 Surface Reconstruction

The computer graphics field has spent considerable effort to develop methodologies for creating representations from sets of data. Generally, these sets of data are acquired from a sensor. Methodologies have progressed steadily and are often designed for a specific application. One of the original motivations was to generate surfaces from medical imaging data. This improves a doctor's decisions because the data are presented in a more intuitive manner. Current applications include augmented reality and 3D printing. Older methodologies were not as concerned with speed and often times had a large computational cost. Also, the methodologies are often designed for single objects or small environments. Following the taxonomy of such well known works as [54, 55], the field can be roughly divided into representations that are generated with volume-based techniques and those that use surface-based techniques. Methods that use volume-based techniques are characterized by spatially subdividing the environmental volume and are usually computationally expensive and require a large amount of memory. Methods that use surface-based techniques generate the representation using surface properties of the input data. Both types

of methods can have mechanisms to adapt the mesh to noisy or new information. In the following section we will trace the progression of the methodologies.

2.2.1 Volume-based

Volume-based methods have the characteristic of spatially subdividing the volume into smaller parts. One of the first well known works that used a volume-based technique was proposed by Lorensen and Cline in 1987 [3]. In this work they proposed a method named marching cubes, which is still known for its reliability and simplicity and is used by applications that do not have a computational requirement. Marching cubes subdivides the space into cubes. The data contained in each cube dictate how the surface connectivity will be defined in that cube. Possible vertex locations are at the corners and along the edges. Once this has been done for all cubes the process is complete. One of the next major steps came from Hoppe et al. in 1992 [56] In this work they used the input points to define a Signed Distance Function (SDF) in 3D space and then meshed the zero-set to obtain the output mesh. A SDF is a spatial function that has the value of the distance to the nearest surface at each point. The sign is used to specify if the point is inside or outside of the surface relative to the sensor. The zero-set of the SDF is the surface where the values transition from positive to negative. Using a SDF has proven to be very effective and has been the core idea of many methodologies that came after this work of Hoppe et al., such as KinectFusion [6]. One of the next advances came from Edelsbrunner and Mücke in 1994 [57] with a method named alpha shapes. They used 3D Delaunay triangulation and the input point set to decompose the volume into a Delaunay tetrahedrization. This gives a triangulation of the input set which involves all points. A sphere of radius alpha is then used to remove edges and vertices to obtain a mesh of user specified resolution. Many works have made use of 3D Delaunay triangulation to create a mesh. Methods which use 3D Delaunay on the input set have a large computational

cost and often cannot be executed in real-time. The next valuable contribution came from Bloomenthal in 1994 [58] as open source software for surface polygonization of implicit functions. This was a stable and robust open source software that has been used in many well-known algorithms [45]. Another major advance came from Curless and Levoy in 1996 [59]. In this work they also constructed a Truncated Signed Distance Function (TSDF). A TSDF is very similar to a SDF; the only difference is that distance values are truncated after they exceed a threshold. Their method was one of the first to be able to handle several registered range scans. Their work showed how well a TSDF can deal with several noisy scans by naturally integrating out the noise. They obtained very good results but were not even close to real-time. A speed up in processing time was achieved by Pulli et al. in 1997 [60] by utilizing octrees. They obtained good results and their method was used by Surmann et al. [61] in a well-known robotic mapping work. Another major advance came in 2001 from Zhao et al [62]. They used Partial Differential Equation (PDE) methods to obtain a final reconstruction that was of better quality than prior methods. In 2001 Carr et al. [63] created a volumetric method based on the radial basis function (RBF). Their method was able to successfully deal with holes and generate water tight models. A water tight model is useful for single object reconstruction. However, it is not desired for mapping large environments. One of the next major advances was published in 2003 by Ohtake et al. [46]. In this work they created a method that was faster than the work of Carr et al. [63] by implementing a hierarchical approach with compactly supported basis functions. At the time, their work was considered to be the state of the art for calculating an implicit function of a noisy point set and was used by Newcombe et al. [45]. Volume-based methods have been able to create high quality representations and work well for single objects and small environments. These methods must spatially divide the environmental volume and therefore have a high memory requirement.

2.2.2   Surface-based

One of the first interesting and adaptive surface-based methods was published by Terzopoulos and Vasilescu in 1991 [64] and dealt with 2.5D data such as intensity and range images. The goal of their work was to create an adaptive mesh of an input image. The mesh was initialized as a 2D sheet of mesh elements with virtual springs along each edge. The stiffness of each virtual spring would then adjust based on the image information at its locations. The mesh was able to adapt to be more dense in regions of higher intensity. In 1992 Terzopoulos and Vasilescu extended their methodology to 3D data [65]. In this work they used the distance between the mesh and the data to drive the vertices to be near the surface. In this early work they needed to initialize the mesh and control the subdivision of mesh elements to obtain a suitable resolution. In 1993 Hoppe et al. [66] published a method that used an energy minimization framework. Their method minimized an energy function that modeled the competing desires of conciseness of representation and fidelity to the data. They successfully used their method for both surface reconstruction and mesh simplification. One of the next advances in physical based adaptation of meshes came in 1993 from Huang and Goldof [67]. In this work they were able to adjust the size of the mesh elements to obtain a denser resolution in areas of high frequency information using a physical based model. In addition, it was one of the first works to represent an object undergoing deformation. Their method was able to perform tracking on simple simulation examples. Another advancement came in 1994 Rutishauser et al. [68] with a method specifically designed for incremental data. Their methodology worked with a sequential input set of range data and used a probabilistic framework to adjust the vertices of a mesh to the expected value given the prior observations. Their methodology also modeled the noise of the sensor with a sensor model. In 1994 Delingette [69] developed a methodology to generate a simplex mesh model of structured and unstructured 3D datasets. Elastic behavior of the mesh surface

was modeled by local stabilizing functionals. Also, they implemented an iterative refinement process to refine the mesh in areas of high frequency information. One of the next steps was published by Turk and Levoy in 1994 [70]. Their method allowed overlapping meshes to be "zippered" into a single mesh surface. This ability is especially important for methods that generate a mesh for each depth image of the sensor and then need to combine all registered meshes into a single mesh. Their method is computationally expensive due to distance calculations. An interesting work came in 1995 from Chen and Medioni [71]. They devised an adaptive mesh methodology based on the inflation of a balloon. A mesh sphere was first initialized within the registered range measurements of the object. Virtual inflation forces were then used to expand the balloon until the mesh surface was a minimal distance from the range data. This method was limited to objects that are water tight. A major advancement came in 1999 from Bernardini et al., [72] in a method named the ball-pivoting algorithm. Their method is a good example of an advancing front method. These types of algorithms start with a seed mesh element and advance the boundary by adding new mesh elements in the immediate area of the boundary which is supported by measurements. Advancing front algorithms differ in how it is decided to add new mesh elements. In the work of Bernardini et al., a virtual sphere of a user defined radius is rolled along the boundary of the mesh and new elements are added if the ball touches another measurement. Their methodology became popular because of its simplicity. One major disadvantage was that the generated mesh was a fixed topology. Another advancing front method came in 2001 from Gopi et al. [73, 54]. Here, they sampled the input dataset to obtain a new dataset with a lower density of points in areas of lower frequency information. This effectively gave their method an adaptive topology. Next, a local neighborhood was computed at each data point and projected to a plane tangent to the surface. The triangulation is then computed on this local tangent plane. They obtained impressive results on datasets of varying sample density and curvature. An interesting work was published in 2003 by Ivris-

simtzis et al. [74]. Here they used a neural network model to adapt a mesh model to the data. They claimed that their method is computationally independent of the size of the input dataset because the dataset is only sampled by the method. There obtained good results. In 2004 Alexa et al. published a very interesting work to generate point set surfaces from an input dataset [75]. They use moving least squares (MLS) to locally approximate the surface with polynomials. The original dataset is then no longer used. Instead, they develop tools to sample the approximated surface to any resolution desired so that the end result is another point set of user specified resolution lying closer to the surface than the input dataset. One drawback is they had to develop their own methodology to render a point set. In 2005 Scheidegger et al. used the work of Alexa et al. to develop an advancing front methodology to generate concise meshes of high accuracy. Their main contribution was to augment an advancing front algorithm with global information so that the triangle size could adapt gracefully to any change. They obtained very impressive results. Most methodologies in Surface Reconstruction had been solely concerned with object or small environment recreation and have computational or memory requirements that do not work well with large environments. One of the first successful methods intended for large environments was published in 2009 by Marton et al. [76]. Their methodology was an advancing front algorithm that worked on a point set sampled from the MLS surface of the original point set. They were able to obtain impressive and near real-time results on datasets of large environments. They also developed a method to deal with revisited parts of the scene by determining the overlapping area and reconstructing only the updated part of the surface mesh. To support dynamic scenes they developed mechanisms to decouple and reconstruct the mesh quickly. They only discussed these mechanisms in theory and had no results of how these mechanisms work.

2.3   Summary

The fields of Robotics and Computer Vision have developed many exciting methodologies to construct representations from a noisy input dataset. However, there is still work to be done to obtain the ideal reconstruction method. A mesh is clearly a desirable type of representation. An ideal method both generates and maintains a mesh representation efficiently. Also, many existing methods do not leverage the inherent structural information contained within the depth image. There are imaging processing techniques that could be used to answer some of the remaining problems in surface reconstruction, such as the need for adaptive topology and the need to decide how each measurement should be used to update the existing mesh. Henry et al. [48] have already investigated using the difference between the expected and actual measurements to guide the decision of how to use each measurement. However, their work was intended for surfels and needs to be extended to meshes. A method to generate a representation is needed which is computationally and memory efficient and can adapt the representation to new information.

Chapter 3

Approach

3.1 Algorithmic Design

The algorithmic structure of MABDI can be seen in the system diagram shown in Fig. 3.1. Table 3.1 gives a description of the main variables.

Table 3.1: Description of the main variables

Variable Name	Description
D	Depth image from RGB-D sensor
P	Pose of the sensor
D_n	Parts of D that are *novel*
S	Novel surface generated from D_n
M	Global mesh

The system diagram of Fig. 3.1 is a more detailed version of the diagram seen in Fig. 1.2b. The "Identify Novel Data" component, shown in Fig. 1.2b, corresponds with the Classification component, shown in blue. This Classification component is MABDI's contribution to the state-of-art in mesh based mapping algorithms, and is what gives MABDI the ability to make decisions about the incoming data. The
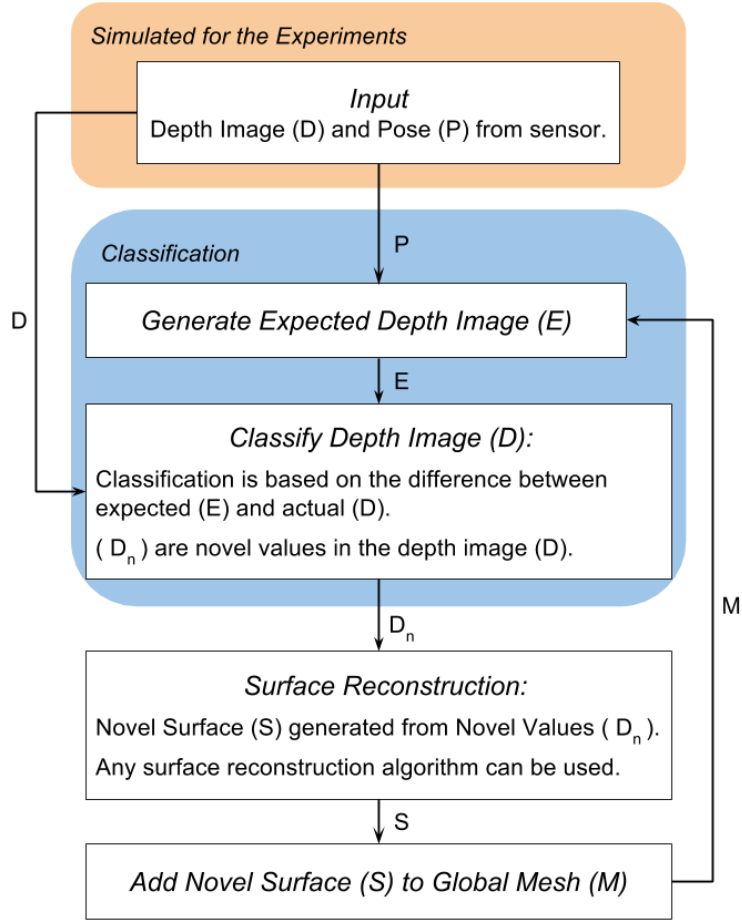
Figure 3.1: MABDI system diagram

Classification component consists of two parts:

1. *Generate Expected Depth Image E* - Here we take the global mesh M, render it using computer graphics, and use the depth buffer of the render window to create a depth image E of what we expect to see from our sensor. This method requires the current pose P of the actual sensor (simulated for our experiments).

2. *Classify Depth Image D* - Here we classify the actual depth image D (simulated

for our experiments) by first taking the absolute difference between E and D and thresholding, as shown in the equation below. If the differences are small, those points are thrown away and if the differences are large, those points are kept as D_n. The idea behind this is, if the difference is large, the measurements are coming from a part of the environment that has not been seen before, i.e. novel. We found $threshold=0.01$ worked well in our simulations. The implication of assuming all large differences signifies novel data is that this version of MABDI cannot handle object removal. It is worth noting that MABDI can be extended to handle object removal by using the sign of the difference between E and D instead of the absolute value.

$$D_n = |D - E| > threshold$$

The system diagram in Fig. 3.1 also shows the Input and the Surface Reconstruction components. The Input component has been simulated for our experiments. More details of this simulation will be covered in Chapter **??**. The Surface Reconstruction component of the MABDI algorithm can be implemented with any viable surface reconstruction method. Our implementation utilizes the structural information contained within the depth image. We will discuss this in more detail in the next section.

3.2 Implementation

3.2.1 Surface Reconstruction

The Surface Reconstruction component, as shown in Fig. 3.1, is responsible for creating a surface S from the novel points D_n. The surface S is a mesh data structure that consists of a list of vertices and elements. Vertices are points and elements define

connections between vertices. Our method outputs a triangle mesh, and so elements define the connection between three vertices. D_n is a subset of D and is a list of pixel locations. For this discussion, it will also be useful to define D_k as the set of pixels in D that are not pixels of D_n, shown in the equation below. D_{known} is labeled with "*known*" because it represents data from the not novel or "known" parts of the environment.

$$D_{known} = D \setminus D_n$$

Our surface reconstruction method first defines S using all pixels from D. We define the topology of the elements on the depth image. We can do this because a depth image is not a set of unorganized points, but has inherent structural information. This characteristic of the depth image allows us to define a topology on the 2D depth image that is preserved when projected to 3D coordinates. The topology we define can be visualized in Fig. 3.2. Elements of the mesh are shown in light blue and pixels from D are shown as blue dots. Next we will identify elements to remove from S.

In order to remove elements defined by points that lie on completely different surfaces, we use an imaging technique in the form of a convolution filter. A two dimensional, differencing convolution filter is passed over D. This filter has a magnified response at points where the difference between neighboring pixels is large. Remembering pixel values signify depth, it is assumed pixels with large differences between themselves and their neighbor lie on different surfaces and therefore lie on the "boundary" of the real surface. A large difference is defined by thresholding on the result of the convolution. We found $threshold$=0.01 worked well in our simulations. Pixels identified through this thresholding are marked as $D_{boundary}$ and are defined by the equation below.
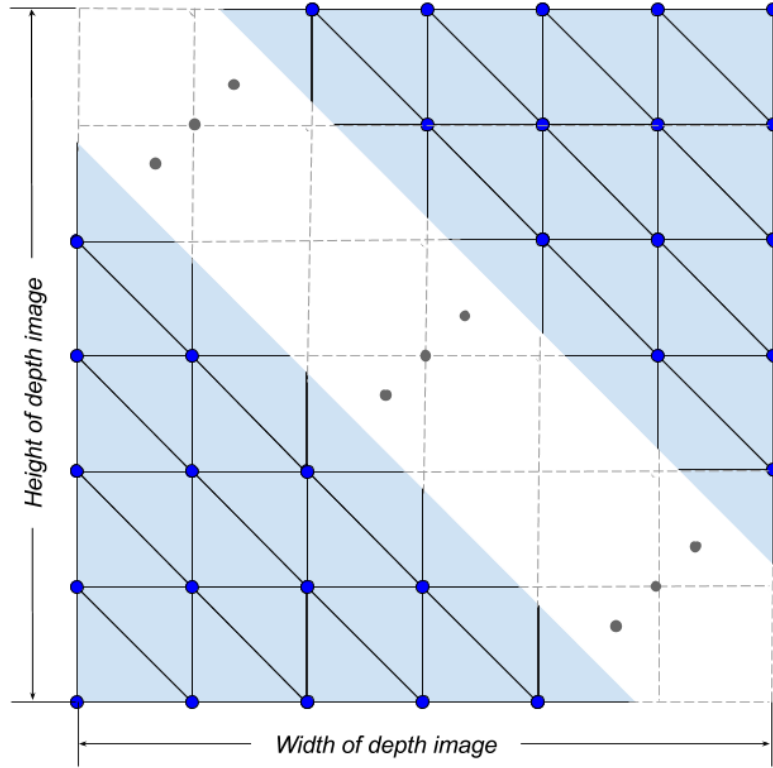
Figure 3.2: Topology defined on the depth image (not all elements are shown)

$$D_{boundary} = D * \begin{bmatrix} 2 & -1 \\ -1 & 0 \end{bmatrix} > threshold$$

Elements are removed from the S if they touch pixels from the sets:

- D_{known} - Pixels from the known parts of the environment.

- $D_{boundary}$ - Pixels that lie on the boundary of the actual surface.

- $D_{invalid}$ - Pixels that are invalid measurements. The RGB-D sensor naturally has pixels that are invalid, for example, those that are out of range.

Let us combine the sets defined above into one set $D_{throwaway}$:

$$D_{throwaway} = D_{known} \cup D_{boundary} \cup D_{invalid}$$

Our method removes elements that contain pixels from the set $D_{throwaway}$. This can be seen in Fig. 3.3. Red dots signify pixels from $D_{throwaway}$ and elements that contain these pixels are removed from S. In the final step, all pixels are projected into 3D coordinates using the transformation matrix of the sensor. These coordinates are the vertices of S.
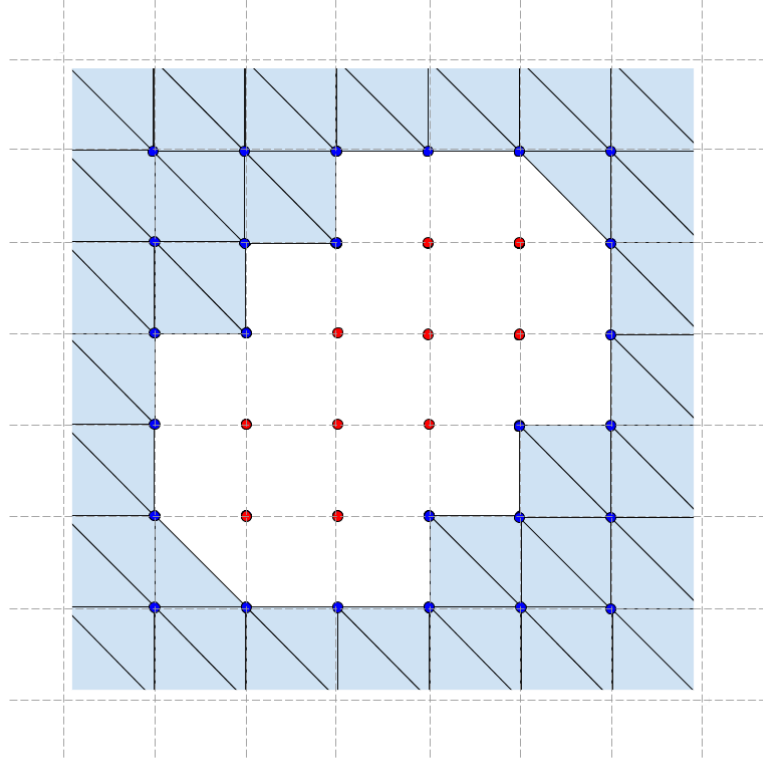

Figure 3.3: Removal of elements

Our surface reconstruction method was chosen for its ability to be implemented simply and run quickly. One consequence of our method is that the resulting surface S can have a large number of elements. For example, if no points are contained in

the set $D_{throwaway}$ (this can happen on the first frame), S will contain over 600,000 elements. We can see this by looking at Fig. 3.2, assuming a depth image of size 640×480, and considering the equation below.

$$613,120 = (2 \times 640) \times (480 - 1)$$

Many surface reconstruction methods have been developed to create a surface more intelligently, as discussed in Chapter 2. For example, the advancing front method developed by Marton et al. [76] is capable of creating surfaces with fewer elements than our method by utilizing a robust resampling method. One great thing about the MABDI algorithm is that the method developed by Marton et al. can be used in place of our surface reconstruction method. This characteristic of MABDI is great because MABDI does not depend on the choice of surface reconstruction method and the method can be chosen as the state-of-the-art changes or to suit a particular application. Also, due to our implementation's modular software design, the entire code base would not need to be changed in order to accomplish this. We will discuss the software design in the next section.

3.2.2   Software Design

From a software perspective, the major difficulty of implementing the MABDI algorithm was found to be creating both the simulated depth image D and the expected depth image E. In addition, managing the complexity of the data pipeline needed to run the algorithm and the simulation of the sensor proved to be difficult. Thankfully, Kitware, which is a leading edge developer of open-source software, created the Visualization Toolkit (VTK) [77, 78]. At the time of this writing the VTK Github repository has over 60,000 commits and is contributed to by supporters such as Sandia National Labs [79].

VTK is suitable for the implementation of MABDI for many reasons. Perhaps the most important is the concept of a vtkAlgorithm (often called a Filter). This allows a programmer to create a custom and modular processing pipeline by defining classes that inherit vtkAlgorithm and then defining the connections between these classes. For example, you could have a pipeline that reads an image from a source (component 1), performs edge detection (component 2), and then renders the image (component 3).

Using the concept of VTK filters, the individual elements of MABDI can be succinctly defined in individual classes. With that in mind, we can see in Fig. 3.4 the layout used in our implementation of MABDI. vtkImageData and vtkPolyData are VTK types used to represent an image and mesh respectively. The elements shown in blue in Fig. 3.4 are the core components of the MABDI algorithm and are implemented as custom VTK filters. Their source code is included in Appendix A. Here we will discuss all components in detail:

- *Source* - Classes with the prefix Source define the environment that is used for the simulation and provide a mesh in the form of a vtkPolyData.

- *FilterDepthImage* - Render the incoming vtkPolyData in a window and output the depth buffer from the window as a vtkImageData. The output additionally has pose information of the sensor.

- *FilterClassifier* - Implements the true innovation of MABDI, i.e., takes the difference between the two incoming depth images (vtkImageData) and outputs a new depth image where the data that is not novel is marked to be thrown away.

- *FilterDepthImageToSurface* - Performs surface reconstruction on the novel points. For more detail see Section 3.2.1. The surface is output as a vtkPoly-Data.

- *FilterWorldMesh* - Here we simply append the incoming novel surface to a growing global mesh that is also output as a vtkPolyData.

MABDI is implemented in Python and uses VTK. Our implementation is distributed under the BSD license and is available on Github at the address below:

$$https://github.com/lucasplus/MABDI$$

At the time of this writing, it consists of over 1,400 lines. The code that implements the MABDI algorithm itself is around 750 lines.
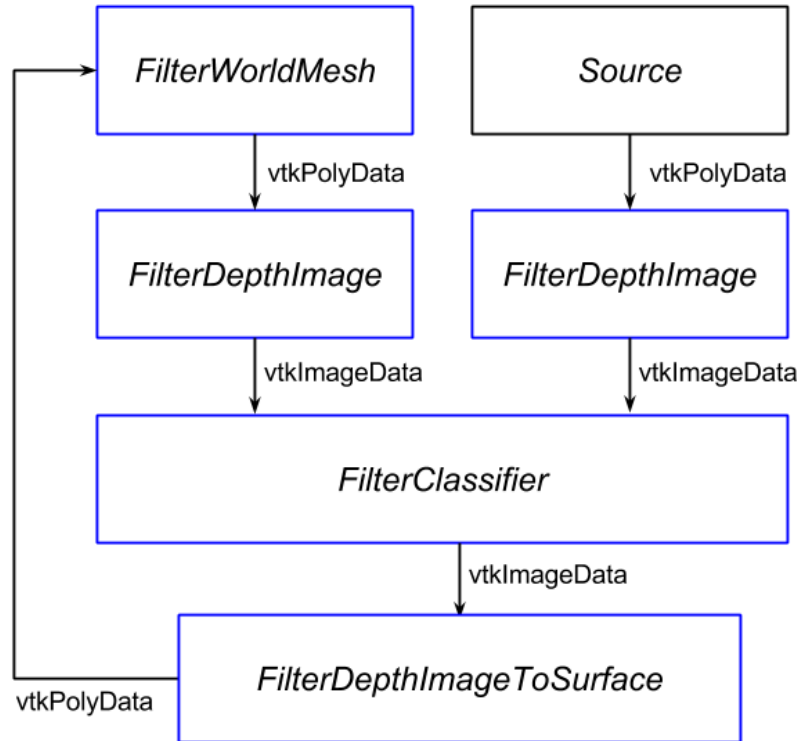
Figure 3.4: MABDI software diagram

Appendix A

MABDI code

A.1   FilterDepthImage.py

FilterDepthImage.py

```python
import vtk
from vtk.util.vtkAlgorithm import VTKPythonAlgorithmBase
from vtk.util import numpy_support
from vtk.numpy_interface import dataset_adapter as dsa


import numpy as np


from timeit import default_timer as timer
import logging


class FilterDepthImage(VTKPythonAlgorithmBase):
    """
    Create a depth image of a scene

    This class uses the geometric information of the scene (vtkPolyData) and the
    orientation of the depth sensor.
    """

    def __init__(self,
```

```python
21                      name='none',
22                      offscreen=False,
23                      noise=0.0,
24                      depth_image_size=(640, 480)):
25          """
26          :param name: default='none'
27            Used for the logging statements.
28          :param offscreen:
29            Create the render window that is used to produce the depth image offscreen
       .
30          :param noise:
31            Noise to add to depth image.
32          :param depth_image_size:
33            Size of the depth image.
34          """
35
36          VTKPythonAlgorithmBase.__init__(self,
37                                          nInputPorts=0,
38                                          nOutputPorts=1, outputType='vtkImageData')
39          self._name = name
40
41          if type(noise) == bool:
42              if noise:
43                  noise = 0.002
44              else:
45                  noise = 0.0
46          self._noise = noise
47
48          # vtk render objects
49          self._ren = vtk.vtkRenderer()
50          self._renWin = vtk.vtkRenderWindow()
51          self._iren = vtk.vtkRenderWindowInteractor()
52
53          # wire them up
54          self._renWin.AddRenderer(self._ren)
55          self._iren.SetRenderWindow(self._renWin)
56
57          # offscreen rendering
58          if offscreen:
59              self._renWin.SetOffScreenRendering(1)
60
61          # kinect intrinsic parameters
62          # https://msdn.microsoft.com/en-us/library/hh438998.aspx
```

```python
63              self._renWin.SetSize(depth_image_size)
64              self._ren.GetActiveCamera().SetViewAngle(60.0)
65              self._ren.GetActiveCamera().SetClippingRange(0.8, 4.0)
66              self._iren.GetInteractorStyle().SetAutoAdjustCameraClippingRange(0)
67
68              # have it looking down and underneath the "floor"
69              # so that it will produce a blank vtkImageData until
70              # set_sensor_orientation() is called
71              self._ren.GetActiveCamera().SetPosition(0.0, -20.0, 0.0)
72              self._ren.GetActiveCamera().SetFocalPoint(0.0, -25.0, 0.0)
73
74              # calculate image bounds
75              self._imageBounds = [0, 0, 0, 0]
76              viewport = self._ren.GetViewport()
77              size = self._renWin.GetSize()
78              self._imageBounds[0] = int(viewport[0] * size[0])
79              self._imageBounds[1] = int(viewport[1] * size[1])
80              self._imageBounds[2] = int(viewport[2] * size[0] + 0.5) - 1
81              self._imageBounds[3] = int(viewport[3] * size[1] + 0.5) - 1
82
83          def set_polydata(self, in_polydata):
84              """
85              What this filter will render and consequently produce a depth image of.
86              :param in_polydata: vtkAlgorithm that produces a vtkPolyData
87              """
88              logging.info('')
89
90              mapper = vtk.vtkPolyDataMapper()
91              mapper.SetInputConnection(in_polydata.GetOutputPort())
92
93              actor = vtk.vtkActor()
94              actor.SetMapper(mapper)
95
96              self._ren.AddActor(actor)
97
98              self._iren.Initialize()
99              self._iren.Render()
100
101         def set_polydata_empty(self):
102             """
103             Use to initialize this filter with an empty vtkPolyData
104             """
105             logging.info('')
```

```python
106
107            polydata = vtk.vtkPolyData()
108
109            mapper = vtk.vtkPolyDataMapper()
110            mapper.SetInputDataObject(polydata)
111
112            actor = vtk.vtkActor()
113            actor.SetMapper(mapper)
114
115            self._ren.AddActor(actor)
116
117            self._iren.Initialize()
118            self._iren.Render()
119
120        def set_sensor_orientation(self, in_position, in_lookat):
121            """
122            :param in_position: Position of sensor in world coordinates.
123            :param in_lookat: Where the sensor is looking in world coordinates.
124            """
125            logging.info('position{} lookat{}'.format(in_position, in_lookat))
126
127            self._ren.GetActiveCamera().SetPosition(in_position)
128            self._ren.GetActiveCamera().SetFocalPoint(in_lookat)
129            self._iren.Render()
130
131        def get_vtk_camera(self):
132            return self._ren.GetActiveCamera()
133
134        def get_width_by_height_ratio(self):
135            return float(self._renWin.GetSize()[0]) / float(self._renWin.GetSize()[1])
136
137        def kill_render_window(self):
138            """
139            Kill render window that this instance owns. Only to be used when the user
140            is sure the filter will not be run again.
141            """
142            # http://stackoverflow.com/questions/15639762/close-vtk-window-python
143            self._renWin.Finalize()
144            self._iren.TerminateApp()
145            del self._renWin, self._iren
146
147        def RequestInformation(self, request, inInfo, outInfo):
148            logging.info('')
```

```python
149            size = self._renWin.GetSize()
150            extent = (0, size[0] - 1, 0, size[1] - 1, 0, 0)
151            info = outInfo.GetInformationObject(0)
152            info.Set(vtk.vtkStreamingDemandDrivenPipeline.WHOLE_EXTENT(),
153                     extent, len(extent))
154            return 1
155
156        def RequestData(self, request, inInfo, outInfo):
157            logging.info('{}'.format(self._name))
158            start = timer()
159
160            # get the depth values
161            vfa = vtk.vtkFloatArray()
162            ib = self._imageBounds
163            self._renWin.GetZbufferData(ib[0], ib[1], ib[2], ib[3], vfa)
164
165            # add noise
166            if self._noise is not 0.0:
167                nvfa = numpy_support.vtk_to_numpy(vfa)
168                nvfa += self._noise * nvfa * np.random.normal(0.0, 1.0, nvfa.shape)
169                vfa = dsa.numpyTovtkDataArray(nvfa)
170
171            # pack the depth values into the output vtkImageData
172            info = outInfo.GetInformationObject(0)
173            ue = info.Get(vtk.vtkStreamingDemandDrivenPipeline.UPDATE_EXTENT())
174            out = vtk.vtkImageData.GetData(outInfo)
175            out.GetPointData().SetScalars(vfa)
176            out.SetExtent(ue)
177
178            # append meta data to the vtkImageData containing intrinsic parameters
179            out.sizex = self._renWin.GetSize()[0]
180            out.sizey = self._renWin.GetSize()[1]
181            out.viewport = self._ren.GetViewport()
182            vtktmat = self._ren.GetActiveCamera().GetCompositeProjectionTransformMatrix(
183                self._ren.GetTiledAspectRatio(),
184                0.0, 1.0)
185            vtktmat.Invert()
186            out.tmat = self._vtkmatrix_to_numpy(vtktmat)
187
188            end = timer()
189            logging.info('Execution time {:.4f} seconds'.format(end - start))
190
191            return 1
```

```
192
193     def _vtkmatrix_to_numpy(self, matrix):
194         """
195         Copies the elements of a vtkMatrix4x4 into a numpy array.
196
197         :param matrix: The matrix to be copied into an array.
198         :type matrix: vtk.vtkMatrix4x4
199         :rtype: numpy.ndarray
200         """
201         m = np.ones((4, 4))
202         for i in range(4):
203             for j in range(4):
204                 m[i, j] = matrix.GetElement(i, j)
205         return m
```

A.2   FilterClassifier.py

FilterClassifier.py

```
1   import vtk
2   from vtk.util.vtkAlgorithm import VTKPythonAlgorithmBase
3   from vtk.util import numpy_support
4
5   from timeit import default_timer as timer
6   import logging
7
8
9   class FilterClassifier(VTKPythonAlgorithmBase):
10      """
11      vtkAlgorithm with 2 inputs of vtkImageData and an output of vtkImageData
12      Input: Depth images
13      Output: Classified depth image
14      """
15
16      def __init__(self, param_classifier_threshold=0.01):
17          """
18          :param param_classifier_threshold: default=0.01
19            Threshold to determine when the difference in the depth images is too big
20            and is therefore a novel measurement.
21          :return:
```

```
22          """
23
24          VTKPythonAlgorithmBase.__init__(self,
25                                          nInputPorts=2, inputType='vtkImageData',
26                                          nOutputPorts=1, outputType='vtkImageData')
27
28          self._param_classifier_threshold = param_classifier_threshold
29
30          self._postprocess = []
31          self._postprocess_im1 = []
32          self._postprocess_im2 = []
33          self._postprocess_difim = []
34
35      def set_postprocess(self, do_postprocess):
36          self._postprocess = do_postprocess
37
38      def get_depth_images(self):
39          """
40          Get the depth images. User has to call set_postprocess(True) first.
41          :return: Depth images
42            return[0] - actual
43            return[1] - expected
44            return[2] - threshold absolute difference
45          """
46          return self._postprocess_im1, self._postprocess_im2, self._postprocess_difim
47
48      def RequestInformation(self, request, inInfo, outInfo):
49          logging.info('')
50
51          # input images dimensions
52          info = inInfo[0].GetInformationObject(0)
53          ue1 = info.Get(vtk.vtkStreamingDemandDrivenPipeline.UPDATE_EXTENT())
54          info = inInfo[1].GetInformationObject(0)
55          ue2 = info.Get(vtk.vtkStreamingDemandDrivenPipeline.UPDATE_EXTENT())
56          if ue1 != ue2:
57              logging.warning('Input images have different dimensions. {} {}'.format(
        ue1, ue2))
58
59          extent = ue1
60          info = outInfo.GetInformationObject(0)
61          info.Set(vtk.vtkStreamingDemandDrivenPipeline.WHOLE_EXTENT(),
62                   extent, len(extent))
63
```

```python
64            return 1

66        def RequestData(self, request, inInfo, outInfo):
67            logging.info('')
68            start = timer()

70            # in images (vtkImageData)
71            inp1 = vtk.vtkImageData.GetData(inInfo[0])
72            inp2 = vtk.vtkImageData.GetData(inInfo[1])

74            # convert to numpy arrays
75            dim = inp1.GetDimensions()
76            im1 = numpy_support.vtk_to_numpy(inp1.GetPointData().GetScalars())\
77                .reshape(dim[1], dim[0])
78            dim = inp1.GetDimensions()
79            im2 = numpy_support.vtk_to_numpy(inp2.GetPointData().GetScalars())\
80                .reshape(dim[1], dim[0])

82            # difference in the images
83            # im1 is assumed to be from the actual sensor
84            # im2 is what we expect to see based on the world mesh
85            # Anywhere the difference is small, throw those measurements away
86            # by setting them to one. By doing this FilterDepthImageToSurface
87            # will assume they lie on the clipping plane and will remove them
88            difim = abs(im1 - im2) < self._param_classifier_threshold
89            if self._postprocess:
90                self._postprocess_im1 = im1.copy()
91                self._postprocess_im2 = im2.copy()
92                self._postprocess_difim = difim.copy()
93            imout = im1
94            imout[difim] = 1.0

96            info = outInfo.GetInformationObject(0)
97            ue = info.Get(vtk.vtkStreamingDemandDrivenPipeline.UPDATE_EXTENT())

99            # output vtkImageData
100           out = vtk.vtkImageData.GetData(outInfo)
101           out.SetExtent(ue)
102           (out.sizex, out.sizey, out.tmat, out.viewport) = \
103               (inp1.sizex, inp1.sizey, inp1.tmat, inp1.viewport)
104           out.GetPointData().SetScalars(
105               numpy_support.numpy_to_vtk(imout.reshape(-1)))
106
```

```
107         end = timer()
108         logging.info('Execution time {:.4f} seconds'.format(end − start))
109
110         return 1
```

A.3   FilterDepthImageToSurface.py

FilterDepthImageToSurface.py

```python
1  import vtk
2  from vtk.util.vtkAlgorithm import VTKPythonAlgorithmBase
3  from vtk.util import numpy_support
4  from vtk.numpy_interface import dataset_adapter as dsa
5
6  from Utilities import DebugTimeVTKFilter
7
8  import numpy as np
9  from scipy import ndimage
10
11 from timeit import default_timer as timer
12 import logging
13
14
15 class FilterDepthImageToSurface(VTKPythonAlgorithmBase):
16     """
17     vtkAlgorithm with input of vtkImageData and output of vtkPolyData
18     This filter first defines a connectivity on the depth image that is like a
19     checkerboard but with two triangles in each square. It then throws away all
       points
20     farther than the param_farplane_threshold and all points with a large difference
21     between neighbors (controlled with param_convolution_theshold)
22     Input: Depth image
23     Output: Mesh created by projecting depth image
24     """
25
26     def __init__(self,
27                  param_farplane_threshold=1.0,
28                  param_convolution_threshold=0.01):
29         """
30         Algorithm setup and define parameters.
```

```python
31            :param param_farplane_threshold: default=1.0
32                Values on the depth image range from 0.0-1.0. Points with depth values
      greater
33                than param_farplane_threshold will be thrown away.
34            :param param_convolution_threshold: default=0.01
35                Convolution is used to determine pixel neighbors with a large difference.
      If
36                there is one, the point will be thrown away. This threshold controls
      sensitivity.
37            """
38
39            VTKPythonAlgorithmBase.__init__(self,
40                                            nInputPorts=1, inputType='vtkImageData',
41                                            nOutputPorts=1, outputType='vtkPolyData')
42
43            self._param_farplane_threshold = param_farplane_threshold
44            self.param_convolution_theshold = param_convolution_threshold
45
46            self._sizex = []
47            self._sizey = []
48            self._viewport = []
49
50            self._display_pts = []
51            self._viewport_pts = []
52            self._world_pts = []
53
54            self._points = vtk.vtkPoints()
55            self._polys = vtk.vtkCellArray()
56            self._polydata = vtk.vtkPolyData()
57            self._polydata.SetPoints(self._points)
58            self._polydata.SetPolys(self._polys)
59
60            self._extract = vtk.vtkExtractPolyDataGeometry()
61            DebugTimeVTKFilter(self._extract)
62            self._extract.SetInputData(self._polydata)
63            planefunc = vtk.vtkPlane()
64            planefunc.SetNormal(0.0, -1.0, 0.0)
65            planefunc.SetOrigin(0.0, -1.0, 0.0)
66            self._extract.SetImplicitFunction(planefunc)
67
68        def RequestData(self, request, inInfo, outInfo):
69
70            logging.info('')
```

```python
71          start = timer()
72
73          # input (vtkImageData)
74          inp = vtk.vtkImageData.GetData(inInfo[0])
75
76          # if the vtkImageData size has changed or this is the first time
77          # save new size info and initialize containers
78          if (self._sizex, self._sizey, self._viewport) != (inp.sizex, inp.sizey, inp.
       viewport):
79              (self._sizex, self._sizey) = (inp.sizex, inp.sizey)
80              self._viewport = inp.viewport
81              self._init_containers()
82
83          # the incoming depth image
84          di = numpy_support.vtk_to_numpy(inp.GetPointData().GetScalars())\
85              .reshape((self._sizey, self._sizex))
86
87          # add z values to viewport_pts based on incoming depth image
88          self._viewport_pts[2, :] = di.reshape(-1)
89
90          # project to world coordinates
91          self._world_pts = np.dot(inp.tmat, self._viewport_pts)
92          self._world_pts = self._world_pts / self._world_pts[3]
93
94          """ Remove invalid points """
95
96          # index to pts outside sensor range (defined by vtkCamera clipping range)
97          outside_range = ~(di < self._param_farplane_threshold)
98
99          # find pixel neighbors with large differences in value
100         # http://docs.scipy.org/doc/scipy/reference/tutorial/ndimage.html
101         kh = np.array([[1, -1], [0, 0]])
102         edges_h = abs(ndimage.convolve(di,
103                                         kh,
104                                         mode='nearest',
105                                         origin=-1)) > self.param_convolution_theshold
106         kv = np.array([[1, 0], [-1, 0]])
107         edges_v = abs(ndimage.convolve(di,
108                                         kv,
109                                         mode='nearest',
110                                         origin=-1)) > self.param_convolution_theshold
111
112         # combine all the points found to be invalid
```

Appendix A. MABDI code

```
113            # and set them to a value underneath the "floor of the environment"
114            # http://stackoverflow.com/a/20528566/4068274
115            invalid_index = np.logical_or.reduce((outside_range.reshape(-1),
116                                                  edges_h.reshape(-1),
117                                                  edges_v.reshape(-1)))
118            self._world_pts[0:3, invalid_index] = np.array([[0.0], [-2.0], [0.0]])
119
120            """ Update and set filter output """
121
122            # update vtkPoints
123            vtkarray = dsa.numpyTovtkDataArray(self._world_pts[0:3, :].T)
124            self._points.SetData(vtkarray)
125
126            # update output (vtkPolyData)
127            out = vtk.vtkPolyData.GetData(outInfo)
128            self._extract.Update()
129            logging.info('Number of triangles: {}'.format(self._extract.GetOutput().
        GetNumberOfCells()))
130            out.ShallowCopy(self._extract.GetOutput())
131
132            end = timer()
133            logging.info('Execution time {:.4f} seconds'.format(end - start))
134
135            return 1
136
137    def _init_containers(self):
138            logging.info('Initializing arrays for projection calculation.')
139            tstart = timer()
140
141            # helper variables (width, height)
142            (w, h) = (self._sizex, self._sizey)
143
144            """ display points (list of all pixel coordinates) """
145
146            self._display_pts = np.ones((2, w * h))
147            self._display_pts[0, :], self._display_pts[1, :] = \
148                zip(*[(j, i) for i in np.arange(h) for j in np.arange(w)])
149
150            """ viewport points """
151            # https://github.com/Kitware/VTK/blob/52
        d45496877b00852a08a5b9819d109c2fd9bfab/Rendering/Core/vtkCoordinate.h#L26
152
153            self._viewport_pts = np.ones((4, self._display_pts.shape[1]))
```

42

Appendix A. MABDI code

```python
154            self._viewport_pts[0, :] = 2.0 * (self._display_pts[0, :] - w * self.
        _viewport[0]) / \
155                (w * (self._viewport[2] - self._viewport[0])) - 1.0
156            self._viewport_pts[1, :] = 2.0 * (self._display_pts[1, :] - h * self.
        _viewport[1]) / \
157                (h * (self._viewport[3] - self._viewport[1])) - 1.0
158
159            """ new world points (just initializing the container) """
160
161            self._world_pts = np.ones(self._viewport_pts.shape)
162
163            """ cells (list of triangles created by connecting neighbors in depth image
        space ) """
164
165            # connectivity on the depth image is almost like a checkerboard pattern
166            # except with two triangles in every checkerboard square
167            nt = (2*w)*(h-1)  # number of triangles
168            cells = np.zeros((3, nt), dtype=np.int)
169            i = 0
170            while i < (nt/2):
171                if ((i+1) % w) != 0:  # if on the side of the image skip
172                    cells[:, 2*i] = (i, i+1, w+i)
173                    cells[:, 2*i+1] = (i+1, w+i+1, w+i)
174                i += 1
175
176            # remove columns with zeros (the ones we skipped in the while loop)
177            index = np.where(cells.any(axis=0))[0]  # all columns that are non zero
178            cells = cells[:, index]
179
180            # turn our connectivity list into a vtk object (vtkCellArray)
181            for tpt in cells.T:
182                self._polys.InsertNextCell(3)
183                self._polys.InsertCellPoint(tpt[0])
184                self._polys.InsertCellPoint(tpt[1])
185                self._polys.InsertCellPoint(tpt[2])
186            self._polydata.SetPolys(self._polys)
187
188            # time me
189            tend = timer()
190            logging.info('Initializing arrays for projection calculation {:.4f} seconds'
        .format(tend - tstart))
```

A.4   FilterWorldMesh.py

FilterWorldMesh.py

```python
import vtk
from vtk.util.vtkAlgorithm import VTKPythonAlgorithmBase
from vtk.numpy_interface import dataset_adapter as dsa


import numpy as np
import matplotlib.pyplot as plt


from itertools import cycle


from timeit import default_timer as timer
import logging



class FilterWorldMesh(VTKPythonAlgorithmBase):
    """
    vtkAlgorithm with input vtkPolyData and output vtkPolyData
    Input: Surface to be added to the global mesh
    Output: The global mesh
    """
    def __init__(self, color=False):
        """
        :param color: default=False
          Color every new surface of the global mesh a different color.
        :return:
        """

        VTKPythonAlgorithmBase.__init__(self,
                                        nInputPorts=1, inputType='vtkPolyData',
                                        nOutputPorts=1, outputType='vtkPolyData')

        self._worldmesh = vtk.vtkAppendPolyData()

        # colormap for changing polydata on every iteration
        # http://matplotlib.org/examples/color/colormaps_reference.html
        self._color = color
        if self._color:
            gist_rainbow_r = plt.cm.get_cmap(name='gist_rainbow_r')
            mycm = gist_rainbow_r(range(160, 260, 5))[:, 0:3]
            self._colorcycle = cycle(mycm)
```

Appendix A. MABDI code

```python
40
41      def RequestData(self, request, inInfo, outInfo):
42          logging.info('')
43          start = timer()
44
45          # input polydata
46          # have to make a copy otherwise polys will not show up in the render
47          # even though GetNumberOfCells() says they should be there
48          tmp = vtk.vtkPolyData.GetData(inInfo[0])
49          inp = vtk.vtkPolyData()
50          inp.ShallowCopy(tmp)
51
52          # change color of all cells
53          if self._color:
54              ncells = inp.GetNumberOfCells()
55              c = self._colorcycle.next()
56              vtkarray = dsa.numpyTovtkDataArray(np.tile(c, (ncells, 1)))
57              inp.GetCellData().SetScalars(vtkarray)
58
59          # add to world mesh
60          self._worldmesh.AddInputData(inp)
61          self._worldmesh.Update()
62
63          logging.info('Number of cells: in = {} total = {}'
64                       .format(inp.GetNumberOfCells(),
65                               self._worldmesh.GetOutput().GetNumberOfCells()))
66
67          # output world mesh
68          out = vtk.vtkPolyData.GetData(outInfo)
69          out.ShallowCopy(self._worldmesh.GetOutput())
70
71          end = timer()
72          logging.info('Execution time {:.4f} seconds'.format(end - start))
73
74          return 1
```

References

[1] M. W. Kadous, R. K.-M. Sheh, and C. Sammut, "Effective user interface design for rescue robotics," in *Proceeding of the 1st ACM SIGCHI/SIGART conference on Human-robot interaction - HRI '06*. New York, New York, USA: ACM Press, mar 2006, p. 250.

[2] S. Thrun, "Robotic mapping: A survey," *Exploring artificial intelligence in the new millennium*, no. February, 2002.

[3] W. E. Lorensen and H. E. Cline, "Marching cubes: A high resolution 3D surface construction algorithm," *Computer*, vol. 21, no. 4, pp. 163–169, 1987.

[4] B. Freedman, A. Shpunt, M. Machline, and Y. Arieli, "Depth mapping using projected patterns," 2012.

[5] P. Henry, M. Krainin, E. Herbst, X. Ren, and D. Fox, "RGB-D mapping: Using Kinect-style depth cameras for dense 3D modeling of indoor environments," *The International Journal of Robotics Research*, vol. 31, no. 5, pp. 647–663, apr 2012.

[6] R. A. Newcombe, S. Izadi, O. Hilliges, D. Molyneaux, D. Kim, A. J. Davison, P. Kohli, J. Shotton, S. Hodges, and A. Fitzgibbon, "KinectFusion: Real-time dense surface mapping and tracking," in *2011 10th IEEE International Symposium on Mixed and Augmented Reality, ISMAR 2011*. IEEE, oct 2011, pp. 127–136.

[7] L. Xia, C.-C. Chen, and J. K. Aggarwal, "Human detection using depth information by Kinect," in *CVPR 2011 WORKSHOPS*. IEEE, jun 2011, pp. 15–22.

[8] J. Stowers, M. Hayes, and A. Bainbridge-Smith, "Altitude control of a quadrotor helicopter using depth map from Microsoft Kinect sensor," in *2011 IEEE International Conference on Mechatronics*. IEEE, apr 2011, pp. 358–362.

References

[9] M. Dissanayake, P. Newman, S. Clark, H. Durrant-Whyte, and M. Csorba, "A solution to the simultaneous localization and map building (SLAM) problem," *IEEE Transactions on Robotics and Automation*, vol. 17, no. 3, pp. 229–241, jun 2001.

[10] H. Durrant-Whyte and T. Bailey, "Simultaneous localization and mapping: part I," *Robotics & Automation Magazine*, 2006.

[11] T. Bailey and H. Durrant-Whyte, "Simultaneous localization and mapping (SLAM): Part II," *Robotics & Automation Magazine*, no. September, 2006.

[12] R. Smith, M. Self, and P. Cheeseman, "Estimating uncertain spatial relationships in robotics," *Autonomous robot vehicles*, 1990.

[13] S. Thrun, W. Burgard, and D. Fox, "A Probabilistic Approach to Concurrent Mapping and Localization for Mobile Robots," *Autonomous Robots*, vol. 5, no. 3/4, pp. 253–271, 1998.

[14] J. Gutmann and K. Konolige, "Incremental mapping of large cyclic environments," in *Proceedings 1999 IEEE International Symposium on Computational Intelligence in Robotics and Automation. CIRA'99 (Cat. No.99EX375)*. IEEE, 1999, pp. 318–325.

[15] S. Thrun, D. Fox, W. Burgard, and F. Dellaert, "Robust Monte Carlo localization for mobile robots," *Artificial Intelligence*, vol. 128, no. 1-2, pp. 99–141, may 2001.

[16] M. Montemerlo, S. Thrun, D. Koller, and B. Wegbreit, "FastSLAM: A factored solution to the simultaneous localization and mapping problem," *Proceedings of the National conference on Artificial Intelligence*, pp. 593–598, 2002.

[17] S. Thrun, W. Burgard, and D. Fox, "A real-time algorithm for mobile robot mapping with applications to multi-robot and 3D mapping," in *Proceedings 2000 ICRA. Millennium Conference. IEEE International Conference on Robotics and Automation. Symposia Proceedings (Cat. No.00CH37065)*, vol. 1. IEEE, 2000, pp. 321–328.

[18] Y. Liu and R. Emery, "Using EM to learn 3D models of indoor environments with mobile robots," in *Machine Learning-International Workshop Then Conference*, 2001.

[19] A. Davison, "Real-time simultaneous localisation and mapping with a single camera," in *Proceedings Ninth IEEE International Conference on Computer Vision*. IEEE, 2003, pp. 1403–1410 vol.2.

References

[20] S. Thrun, D. Hahnel, D. Ferguson, M. Montemerlo, R. Triebel, W. Burgard, C. Baker, Z. Omohundro, S. Thayer, and W. Whittaker, "A system for volumetric robotic mapping of abandoned mines," in *2003 IEEE International Conference on Robotics and Automation (Cat. No.03CH37422)*, vol. 3. IEEE, 2003, pp. 4270–4275.

[21] A. Howard, D. Wolf, and G. Sukhatme, "Towards 3D mapping in large urban environments," *2004 IEEE/RSJ International Conference on Intelligent Robots and Systems (IROS) (IEEE Cat. No.04CH37566)*, vol. 1, pp. 419–424, 2004.

[22] D. Cole and P. Newman, "Using laser range data for 3D SLAM in outdoor environments," in *Proceedings 2006 IEEE International Conference on Robotics and Automation, 2006. ICRA 2006.* IEEE, 2006, pp. 1556–1563.

[23] G. Klein and D. Murray, "Parallel Tracking and Mapping for Small AR Workspaces," in *2007 6th IEEE and ACM International Symposium on Mixed and Augmented Reality.* IEEE, nov 2007, pp. 1–10.

[24] L. Paz, P. Pinies, J. Tardos, and J. Neira, "Large-Scale 6-DOF SLAM With Stereo-in-Hand," *IEEE Transactions on Robotics*, vol. 24, no. 5, pp. 946–957, oct 2008.

[25] K. Konolige and M. Agrawal, "FrameSLAM: From Bundle Adjustment to Real-Time Visual Mapping," *IEEE Transactions on Robotics*, vol. 24, no. 5, pp. 1066–1077, oct 2008.

[26] H. Strasdat, J. Montiel, and A. Davison, "Scale drift-aware large scale monocular SLAM," *Proceedings of Robotics: Science and Systems (RSS). Vol. 2. No. 3. 2010*, 2010.

[27] N. Engelhard, F. Endres, and J. Hess, "Real-time 3D visual SLAM with a hand-held RGB-D camera," *Proc. of the RGB-D Workshop on 3D Perception in Robotics at the European Robotics Forum*, no. c, 2011.

[28] S. Rusinkiewicz and M. Levoy, "Efficient variants of the ICP algorithm," in *Proceedings Third International Conference on 3-D Digital Imaging and Modeling.* IEEE Comput. Soc, 2001, pp. 145–152.

[29] B. Yamauchi, A. Schultz, and W. Adams, "Mobile Robot Exploration and Map-Building with Continuous Localization," *Proceedings. 1998 IEEE International Conference on Robotics and Automation (Cat. No.98CH36146)*, vol. 4, no. May, pp. 3715–3720, 1998.

References

[30] A. Schultz and W. Adams, "Continuous localization using evidence grids," in *Proceedings. 1998 IEEE International Conference on Robotics and Automation (Cat. No.98CH36146)*, vol. 4.   IEEE, 1998, pp. 2833–2839.

[31] R. Biswas, B. Limketkai, S. Sanner, and S. Thrun, "Towards object mapping in non-stationary environments with mobile robots," in *IEEE/RSJ International Conference on Intelligent Robots and System*, vol. 1.   IEEE, 2002, pp. 1014–1019.

[32] A. Eliazar and R. Parr, "DP-SLAM 2.0," in *IEEE International Conference on Robotics and Automation, 2004. Proceedings. ICRA '04. 2004*.   IEEE, 2004, pp. 1314–1320 Vol.2.

[33] M. Magnusson, A. Lilienthal, and T. Duckett, "Scan registration for autonomous mining vehicles using 3D-NDT," *Journal of Field Robotics*, vol. 24, no. 10, pp. 803–827, oct 2007.

[34] A. Nüchter, K. Lingemann, J. Hertzberg, and H. Surmann, "6D SLAM3D mapping outdoor environments," *Journal of Field Robotics*, vol. 24, no. 8-9, pp. 699–722, aug 2007.

[35] A. Huang and A. Bachrach, "Visual odometry and mapping for autonomous flight using an RGB-D camera," *Int. Symposium on . . .* , pp. 1–16, 2011.

[36] F. Endres, J. Hess, N. Engelhard, J. Sturm, D. Cremers, and W. Burgard, "An evaluation of the RGB-D SLAM system," in *2012 IEEE International Conference on Robotics and Automation*, vol. 3, no. c, IEEE.   IEEE, may 2012, pp. 1691–1696.

[37] C. Martin and S. Thrun, "Real-time acquisition of compact volumetric 3D maps with mobile robots," in *Proceedings 2002 IEEE International Conference on Robotics and Automation (Cat. No.02CH37292)*, vol. 1.   IEEE, 2002, pp. 311–316.

[38] D. Viejo and M. Cazorla, "Unconstrained 3D-Mesh Generation Applied to Map Building," *Progress in Pattern Recognition, Image Analysis and Applications*, vol. 3287, pp. 161–207, 2004.

[39] F. Cazals and J. Giesen, "Delaunay Triangulation Based Surface Reconstruction : Ideas and Algorithms," *INRIA Rapport de recherche*, no. November, pp. 1–45, 2004.

[40] J. Weingarten and R. Siegwart, "3D SLAM using planar segments," in *2006 IEEE/RSJ International Conference on Intelligent Robots and Systems*.   IEEE, oct 2006, pp. 3062–3067.

References

[41] A. Akbarzadeh, J.-M. Frahm, P. Mordohai, B. Clipp, C. Engels, D. Gallup, P. Merrell, M. Phelps, S. Sinha, B. Talton, L. Wang, Q. Yang, H. Stewenius, R. Yang, G. Welch, H. Towles, D. Nister, and M. Pollefeys, "Towards Urban 3D Reconstruction from Video," in *Third International Symposium on 3D Data Processing, Visualization, and Transmission (3DPVT'06)*.   IEEE, jun 2006, pp. 1–8.

[42] M. Pollefeys, D. Nistér, J.-M. Frahm, A. Akbarzadeh, P. Mordohai, B. Clipp, C. Engels, D. Gallup, S.-J. Kim, P. Merrell, C. Salmi, S. Sinha, B. Talton, L. Wang, Q. Yang, H. Stewénius, R. Yang, G. Welch, and H. Towles, "Detailed Real-Time Urban 3D Reconstruction from Video," *International Journal of Computer Vision*, vol. 78, no. 2-3, pp. 143–167, oct 2007.

[43] M. Sainz, R. Pajarola, and Y. Meng, "Depth-Mesh Objects: Fast Depth-Image Meshing and Warping," *Ukpmc.Ac.Uk*, no. 03, 2003.

[44] J. Poppinga, N. Vaskevicius, A. Birk, and K. Pathak, "Fast plane detection and polygonalization in noisy 3D range images," in *Intelligent Robots and Systems (IROS) 2008*.   Ieee, sep 2008, pp. 3378–3383.

[45] R. A. Newcombe and A. J. Davison, "Live dense reconstruction with a single moving camera," in *2010 IEEE Computer Society Conference on Computer Vision and Pattern Recognition*.   IEEE, jun 2010, pp. 1498–1505.

[46] Y. Ohtake, A. Belyaev, and H. Seidel, "A multi-scale approach to 3D scattered data interpolation with compactly supported basis functions," in *2003 Shape Modeling International*.   IEEE Comput. Soc, 2003, pp. 153–161.

[47] J. Stühmer, S. Gumhold, and D. Cremers, "Real-time dense geometry from a handheld camera," *Pattern Recognition*, pp. 11–20, 2010.

[48] P. Henry, M. Krainin, E. Herbst, X. Ren, and D. Fox, "RGB-D Mapping: Using Depth Cameras for Dense 3D Modeling of Indoor Environments," *The International Journal of Robotics Research*, vol. 31, no. 5, pp. 647–663, feb 2012.

[49] T. Weise, T. Wismer, B. Leibe, and L. Van Gool, "In-hand scanning with online loop closure," *2009 IEEE 12th International Conference on Computer Vision Workshops, ICCV Workshops*, pp. 1630–1637, sep 2009.

[50] H. Pfister, M. Zwicker, J. van Baar, and M. Gross, "Surfels : Surface Elements as Rendering Primitives," in *SIGGRAPH 2000*.   New York, New York, USA: ACM Press, jul 2000, pp. 335–342.

References

[51] T. Whelan, M. Kaess, and M. Fallon, "Kintinuous: Spatially extended kinect-fusion," *RSS Workshop on RGB-D: Advanced Reasoning with Depth Cameras*, p. 7, 2012.

[52] T. Whelan, H. Johannsson, M. Kaess, J. J. Leonard, and J. B. McDonald, "Robust Tracking for Real-Time Dense RGB-D Mapping with Kintinuous," in *ICRA 2013*, no. MIT-CSAIL-TR-2012-031. Computer Science and Artificial Intelligence Laboratory, MIT, sep 2012.

[53] L.-K. Cahier, T. Ogata, and H. Okuno, "Incremental probabilistic geometry estimation for robot scene understanding," in *ICRA 2012*. Ieee, may 2012, pp. 3625–3630.

[54] M. Gopi and S. Krishnan, "A fast and efficient projection-based approach for surface reconstruction," in *SIBGRAPI'02*, 2002, pp. 0–7.

[55] R. Mencl and H. Muller, "Interpolation and approximation of surfaces from three-dimensional scattered data points," *Scientific Visualization Conference, 1997*, 1997.

[56] H. Hoppe, T. DeRose, and T. Duchamp, *Surface reconstruction from unorganized points*. ACM, 1992, no. July 1992.

[57] H. Edelsbrunner and E. P. Mücke, "Three-dimensional alpha shapes," *ACM Transactions on Graphics*, vol. 13, no. 1, pp. 43–72, jan 1994.

[58] J. Bloomenthal, "An Implicit Surface Polygonizer," *In Graphics Gems IV*, pp. 324–349, 1994.

[59] B. Curless and M. Levoy, "A volumetric method for building complex models from range images," in *SIGGRAPH '96*, 1996, pp. 303–312.

[60] K. Pulli, T. Duchamp, H. Hoppe, J. McDonald, L. Shapiro, and W. Stuetzle, "Robust meshes from multiple range maps," in *International Conference on Recent Advances in 3-D Digital Imaging and Modeling*. IEEE Comput. Soc. Press, 1997, pp. 205–211.

[61] H. Surmann, A. Nüchter, and J. Hertzberg, "An autonomous mobile robot with a 3D laser range finder for 3D exploration and digitalization of indoor environments," *Robotics and Autonomous Systems*, vol. 45, no. 3-4, pp. 181–198, dec 2003.

[62] H. Zhao, S. Osher, and R. Fedkiw, "Fast surface reconstruction using the level set method," in *Variational and Level Set Methods in Computer Vision, 2001*, 2001, pp. 0–7.

References

[63] J. C. Carr, R. K. Beatson, J. B. Cherrie, T. J. Mitchell, W. R. Fright, B. C. McCallum, and T. R. Evans, "Reconstruction and representation of 3D objects with radial basis functions," *SIGGRAPH '01*, pp. 67–76, 2001.

[64] D. Terzopoulos and M. Vasilescu, "Sampling and Reconstruction with Adaptive Meshes," in *Computer Vision and Pattern Recognition, 1991. Proceedings CVPR '91.*, 1991.

[65] M. Vasilescu and D. Terzopoulos, "Adaptive meshes and shells: irregular triangulation, discontinuities, and hierarchical subdivision," in *Computer Vision and Pattern Recognition*, no. 1.   IEEE Comput. Soc. Press, 1992, pp. 3–6.

[66] H. Hoppe, T. DeRose, T. Duchamp, J. McDonald, and W. Stuetzle, "Mesh Optimization," in *Proceedings of the 20th annual conference on Computer graphics and interactive techniques*, ser. SIGGRAPH '93, vol. d.   New York, NY, USA: ACM, 1993, pp. 19–25.

[67] W.-C. Huang and D. Goldgof, "Adaptive-size meshes for rigid and nonrigid shape analysis and synthesis," *IEEE Transactions on Pattern Analysis and Machine Intelligence*, vol. 15, no. 6, pp. 611–616, jun 1993.

[68] M. Rutishauser, M. Stricker, and M. Trobina, "Merging range images of arbitrarily shaped objects," *Proceedings of IEEE Conference on Computer Vision and Pattern Recognition CVPR-94*, pp. 573–580, 1994.

[69] H. Delingette, "Simplex meshes: a general representation for 3D shape reconstruction," in *Computer Vision and Pattern Recognition*, 1994, pp. 856–859.

[70] G. Turk and M. Levoy, "Zippered polygon meshes from range images," in *SIGGRAPH '94*.   New York, New York, USA: ACM Press, 1994, pp. 311–318.

[71] Y. Chen and G. Medioni, "Description of Complex Objects from Multiple Range Images Using an Inflating Balloon Model," *Computer Vision and Image Understanding*, vol. 61, no. 3, pp. 325–334, may 1995.

[72] F. Bernardini, J. Mittleman, H. Rushmeier, C. Silva, and G. Taubin, "The ball-pivoting algorithm for surface reconstruction," *IEEE Transactions on Visualization and Computer Graphics*, vol. 5, no. 4, pp. 349–359, 1999.

[73] M. Gopi, S. Krishnan, and C. Silva, "Surface reconstruction based on lower dimensional localized Delaunay triangulation," *Computer Graphics Forum*, vol. 19, no. 3, 2001.

References

[74] I. Ivrissimtzis, W.-K. Jeong, and H.-P. Seidel, "Using growing cell structures for surface reconstruction," *2003 Shape Modeling International.*, vol. 2003, pp. 78–86, 2003.

[75] M. Alexa, J. Behr, D. Cohen-Or, S. Fleishman, D. Levin, and C. Silva, "Point set surfaces," *Proceedings Visualization, 2001. VIS '01.*, pp. 21–537, 2004.

[76] Z. C. Marton, R. B. Rusu, and M. Beetz, "On fast surface reconstruction methods for large and noisy point clouds," in *2009 IEEE International Conference on Robotics and Automation.* IEEE, may 2009, pp. 3218–3223.

[77] W. J. Schroeder, B. Lorensen, and K. Martin, *The Visualization Toolkit*, 4th ed. Kitware, 2006.

[78] Kitware. (2016) VTK The Visualization Toolkit. [Online]. Available: http://www.vtk.org/overview/

[79] S. N. Labs. (2016) SNL Computational Systems and Software Environment. [Online]. Available: http://www.sandia.gov/asc/computational_systems/